Biophysical Journal Volume 94 March 2008 2179–2186

Optical Measurement of Mechanical Forces Inside Short DNA Loops

Hari Shroff,*¶ David Sivak,* Jake J. Siegel,*¶ A. L. McEvoy,*¶ Merek Siu,*¶ Andrew Spakowitz,§ Phillip L. Geissler,*‡¶‖ and Jan Liphardt*†¶

*Biophysics Graduate Group, †Department of Physics, and ‡Department of Chemistry, University of California, Berkeley, California 94720; §Department of Chemical Engineering, Stanford University, Stanford, California 94305; and ¶Physical Biosciences Division and ‖Materials Sciences Division, Lawrence Berkeley National Laboratory, Berkeley, California 94720

ABSTRACT Knowledge of the mechanical properties of double-stranded DNA (dsDNA) is essential to understand the role of dsDNA looping in gene regulation and the mechanochemistry of molecular machines that operate on dsDNA. Here, we use a newly developed tool, force sensors with optical readout, to measure the forces inside short, strained loops composed of both dsDNA and single-stranded DNA. By varying the length of the loops and their proportion of dsDNA, it was possible to vary their internal forces from 1 pN to >20 pN. Surprisingly, internal loop forces changed erratically as the amount of dsDNA was increased for a given loop length, with the effect most notable in the smallest loop (57 nucleotides). Monte Carlo simulations based on the helical wormlike chain model accurately predict internal forces when more than half of the loop is dsDNA but fail otherwise. Mismatches engineered into the double-stranded regions increased flexibility, suggesting that Watson-Crick basepaired dsDNA can withstand high compressive forces without recourse to multibase melts. Fluorescence correlation spectroscopy further excluded transient melting (microsecond to millisecond duration) as a mechanism for relief of compressive forces in the tested dsDNAs. DNA loops with integrated force sensors may allow the comprehensive mapping of the elasticity of short dsDNAs as a function of both sequence and salt.

INTRODUCTION

Acute bending of double-stranded DNA (dsDNA) occurs commonly in biology. Intermediates in prokaryotic transcription initiation (1) often consist of highly strained loops of dsDNA interacting with several proteins. Such DNA looping increases the local concentration of protein, allows distal binding sites to act synergistically, and may decrease noise in statistical occupancy of binding sites (2). Sharply bent DNA is also present in nucleosomes, where 147 basepairs (bp) of DNA are tightly spooled in ~1.7 turns around the octameric histone complex (3). Local bend angles can be as high as 160° over 35 bp, as in the DNA-protein complex formed when the integration host factor protein binds to its dsDNA recognition site (4).

Despite the importance of bent DNA, the magnitude of force required to significantly bend it is unknown. Although extensive experimental and theoretical studies of DNA have revealed the elasticity of kilobase-length DNA chains (5,6), the elasticity of shorter DNA is not as well understood. Recent experimental (7,8) and theoretical studies (9,10) have suggested that dsDNA may be more flexible at small length scales than predicted by the conventional wormlike chain (WLC) model. Cloutier and Widom (7) recently found that DNA of ~100 bp cyclized as much as five orders of magnitude more readily than expected from classical elasticity theory. By contrast, Vologodskii and coworkers (11), who performed similar experiments, found the cyclization efficiency of small DNA molecules to be in good agreement with traditional models of DNA bending, albeit with a shorter assumed persistence length ($l_P \approx 47$ nm) than found in other experiments ($l_P \approx 53$ nm) (6). Thus, the forces that develop in dsDNA as it is mechanically deformed remain to be characterized, especially if it is severely bent on length scales much smaller than its persistence length.

Two main technical difficulties have precluded direct measurement of these forces. First, synthesis of dsDNA loops less than l_P in circumference is nontrivial because the formation of such loops is energetically unfavorable. Such loops have thus far been synthesized primarily by the circular ligation of short dsDNA. This method has been utilized in DNA cyclization experiments (7,12), which probe the frequency of spontaneous fluctuations that bring dsDNA chain ends into close proximity. T4 DNA ligase marks such events by rapidly linking chain ends, resulting in the formation of short double-stranded loops. Because low starting concentrations are necessary for a significant conversion of linear reactants to loops (instead of linear concatemers), however, the absolute concentration of DNA loops produced is often in the subnanomolar range, with decreasing yields for loops of decreasing size.

The second barrier to characterizing the forces needed to acutely bend short DNAs is the lack of good tools to measure internal forces. Conventional force-measuring technologies such as optical tweezers (13) or atomic force microscopy (14) are well suited for measuring tensile forces, not compressive forces, and also are better suited for DNA molecules on the kilobase length scale. Although cyclization assays can provide

Submitted June 6, 2007, and accepted for publication September 28, 2007.

Hari Shroff, David Sivak, and Jake J. Siegel contributed equally to this work.

Address reprint requests to Jan Liphardt, Dept. of Physics, University of California, Berkeley, CA 94720. E-mail: Liphardt@physics.berkeley.edu.

Editor: Kathleen B. Hall.

0006-3495/08/03/2179/08 $2.00

doi: 10.1529/biophysj.107.114413

information on the average length, helical repeat, curvature, and bending and twisting flexibility inside a bent DNA circle (12), they become unfeasible for very short strands of dsDNA and do not directly provide information on the forces experienced within the loop.

Force sensors with optical readout (15) in combination with an enzymatic circularization approach allow us to bypass the difficulties outlined above and to measure the internal force in acutely bent DNA. We previously showed that single-stranded DNA (ssDNA) with a dye at each end can be used to measure forces in the piconewton range via changes in FRET (Förster Resonance Energy Transfer (16)) efficiency, E_{FRET}, as the spring is stretched. If force is applied to the sensor, the distance between the two dyes increases, thus decreasing E_{FRET}. Applying a series of known external forces and measuring the resultant E_{FRET} empirically calibrates the sensor and subsequently makes it possible to optically report forces in the range 0–20 pN (15).

Here, we report E_{FRET} and infer internal forces for ~50 different constructs composed of a loop of ssDNA with two attached fluorophores, annealed to varying lengths of complementary DNA to form a partially ssDNA, partially dsDNA loop. We established the dependence of E_{FRET} and force on loop length and the length of the double-stranded region and found that forces of 2–3 pN develop in DNA loops of 101 bases, whereas forces >20 pN develop if the loop size is reduced to 57 bases. These force and FRET efficiency scales quantitatively match predictions of a simple microscopic model that represents segments of ssDNA and dsDNA as fluctuating elastic filaments. Results from simulation and experiment suggest that dsDNA melting is neither frequent nor long-lived, despite compressive forces exceeding 20 pN.

MATERIALS AND METHODS

Synthesis, purification, and annealing of loop constructs

Dual-fluorophore labeled oligonucleotides of lengths 57, 81, and 101 bases (sequences given in the Supplementary Material) were circularized with CircLigase ssDNA Ligase (CL4115K, Epicentre, Madison, WI). Each oligonucleotide contained a conserved force-sensing region consisting of the same sequence of 10 bases separating the fluorophores Cy3 and Cy5. For the polyethylene glycol (PEG) analog, the 10 intervening bases were replaced with a PEG linker of approximately the same size. It was otherwise identical to the 57-base oligonucleotide and experimentally treated in the same way. Reactions were carried out in 20-μl volumes, combining 300 Units of CircLigase with 50 pmol oligonucleotides and incubating for 1 h at 60°C. The circular ligase was then inactivated by heating the reactants to 80°C for 10 min. The 57-, 81-, and 101-base loops were purified from 18%, 10%, or 8% TBE-Urea PAGE gels, respectively.

For some experiments, the purified, dually labeled loops were annealed to complementary oligonucleotides (sequences available in the Supplementary Material). The 100 nM loops were annealed to 1 μM complementary oligonucleotides in 1× TBE buffer, 50 mM NaCl. Annealing mixtures were cooled from 95°C to 4°C over 3 h (81-, 101-base constructs) or from 80°C to 4°C over 90 min (57-base constructs) and then stored at 4°C.

Not all dsDNA lengths are realizable: the force-sensing region between fluorophores must remain single stranded (at least 12 bases must remain single stranded), and the complementary strand must efficiently anneal (gel-mobility shift assays revealed that the annealing efficiency dropped sharply for complements shorter than ~20 nt (Supplementary Fig. S1, *B* and *C*)). These constraints limited the dsDNA length in each loop to 21–43 bp (57-base loop), 21–67 bp (81-base loop), and 21–87 bp (101-base loop).

Bulk FRET efficiencies

Fluorescence emission spectra for each sample were taken, and E_{FRET} was extracted by dividing the intensities of donor and acceptor dyes as previously described (15,17). E_{FRET} was corrected for incomplete donor labeling and for incomplete annealing (details available in the Supplementary Material). All FRET experiments were done at 25°C. For each construct, the quantum yield of the donor was measured using an analogous construct with only the donor fluorophore (Cy3). In addition, the overlap integral was measured, and combined with the quantum yield measurements, the bulk FRET efficiencies were transformed into a common Förster radius (R_0) basis, referred to as E^*_{FRET}, for the purpose of conversion to forces. (Details of this calculation are given in the Supplementary Material.)

Obtaining forces from FRET data

The original, single-molecule data of Shroff et al. (15) were fit to a three-parameter exponential in Sigmaplot (version 10.0, Systat Software, San Jose, CA), $E_{\mathrm{FRET}} = E_\infty + (E_0 - E_\infty)e^{-\mathrm{F}/\mathrm{F}_{\mathrm{char}}}$ where F is the force (in piconewtons), and the efficiency at infinite force E_∞, the efficiency at zero force E_0, and the characteristic force F_{char} are free parameters. The best-fit values for these parameters were $E_\infty = 0.34$, $E_0 = 0.73$, and $F_{\mathrm{char}} = 4$ pN. This empirical formula was inverted to obtain the force as a function of FRET efficiency. The bulk FRET efficiencies, corrected for variations in R_0, were then used to calculate the forces induced in each construct: $F^* = F_{\mathrm{char}}\ln(E_0 - E_\infty / E^*_{\mathrm{FRET}} - E_\infty)$. Errors in the initial three-parameter fit were propagated to reported errors in forces and FRET efficiencies. Initial single-molecule calibration experiments were done in T50 buffer (15) and bulk fluorescence experiments in 1× TBE, 50 mM NaCl. Control bulk fluorescence experiments indicate no difference in E_{FRET} as measured in the two buffers.

Fluorescence correlation spectroscopy

Fluorescence correlation spectroscopy (FCS) measurements were performed using a custom confocal fluorescence microscope described previously (18), with minor modifications. The pinhole diameter was 75 μm, and the laser power was 5 mW before the objective. Cy3 emission autocorrelation measurements for constructs with Cy3 and Cy5 and for loop constructs containing only Cy3 were performed at room temperature. Samples were diluted to 500 pM in filtered T50 buffer (10 mM Tris, 50 mM NaCl, pH 8.0). FCS measurements were taken for 30 s and averaged over 10 runs. Autocorrelation functions for the two dye constructs were averaged ($N = 3$) and divided by the average of those with one dye construct ($N = 3$).

Monte Carlo simulations

We performed Metropolis Monte Carlo simulations without any free parameters for each of the experimental constructs. DNA was represented as a WLC discretized at the level of a single nucleotide, with ssDNA nucleotides and dsDNA bp distinguished by different contour lengths and persistence lengths. Fluorophores were coarse-grained to single spheres tethered by a 1-nm linker to their ssDNA attachment site. Our Hamiltonian included DNA bending elasticity, twist elasticity, and volume interactions. We sampled thermal fluctuations of model DNA loops using standard Metropolis Monte Carlo methods. Trial displacements preserving geometric constraints included ''crankshaft rotations'' and twist rotations. We calculated E_{FRET} by averaging the standard Förster efficiency formula over the computed equilibrium

distribution of fluorophore separations. Parameters R_0 and ssDNA persistence length (l_P^{ss}) were fit through calibration to previous single-molecule force experiments (details available in the Supplementary Material).

RESULTS AND DISCUSSION

General properties of the strained loops

We synthesized and purified 42 stable constructs consisting of a particular ssDNA loop (57-, 87-, or 101-base loop) annealed to a particular length of complementary ssDNA (Fig. 1 *A*). The flexibility of each construct was tuned by annealing different lengths of complementary DNA to the loop. The bulk E_{FRET} for each of these constructs is shown in Fig. 1 *B*. The variability within a particular FRET measurement was small, and repeated trials on independent samples led to E_{FRET} values that generally agreed to within 0.01 efficiency units. In general, E_{FRET} increased as loop length increased (Fig. 1 *B*), as expected from the entropic elasticity of ssDNA and the distance dependence of E_{FRET}: longer stretches of ssDNA exert larger restoring forces that keep the fluorophores in closer proximity, increasing the efficiency of energy transfer.

Because identical force sensor sequences were used in the previous calibration experiments and in the constructs used here, the induced internal force can be estimated from the measured bulk E_{FRET} by calculating the force using the previous force-efficiency calibration (15) (see also Methods). Because our loop constructs execute substantial fluctuations, force values inferred from calibration measurements are approximations of the average forces experienced by the sensor region. Specifically, a force calculated in this way represents the single value of tension on the sensor region that would yield the same average E_{FRET} as observed for the fluctuating loop. To the extent that E_{FRET} is a convex function of tension in our previous single-molecule experiments, the force values we report underestimate actual ensemble averages. Monte Carlo simulations suggest a magnitude of ~1–5 pN for this systematically downward bias (Supplementary Material and Fig. S2).

On conversion of each E_{FRET} to a force, we found that a maximum internal force >20 pN was induced in the smallest loop, whereas the largest loop we examined had a maximum induced internal force of only 3.1 ± 0.9 pN (Fig. 1 *C*).

Detailed properties of the strained loops

We next examined the detailed behavior of E_{FRET} as a function of loop length and dsDNA length (Fig. 2 *A*). As expected, for a fixed dsDNA length (e.g., 35 bp), E_{FRET} increased with loop length. However, for a given loop length (e.g., 57 bases) the E_{FRET}-versus-dsDNA length relationship was unexpectedly complex. Basic, but incomplete, mechanical considerations imply that increasing the dsDNA length within a given loop length should monotonically reduce E_{FRET} because such an increase in dsDNA length ought to be accompanied by an increase in overall stiffness in the loop.

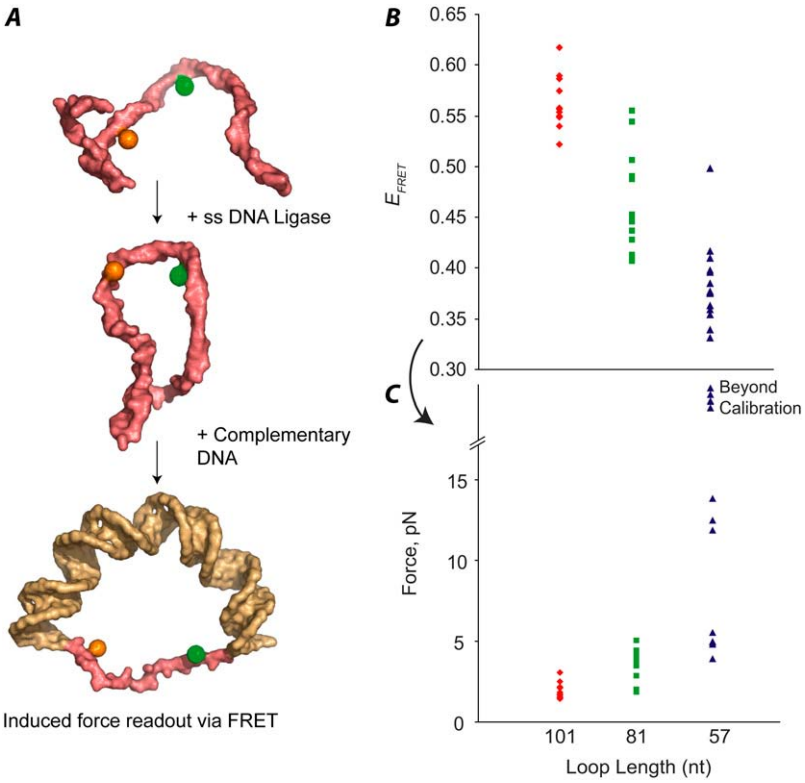

FIGURE 1 (*A*) Experimental schematic. ssDNA oligos containing force sensors are circularized with a single-stranded ligase. Variation of internal force is achieved by annealing different lengths of complementary DNA to the loops. FRET allows readout of the forces induced in the loop. Circles, FRET dyes; pink, ssDNA; gold, dsDNA. (*B*) E_{FRET} for three different loop lengths, annealed to a variety of complement lengths. Each point corresponds to a distinct construct. (*C*) Forces corresponding to the data in *B* after correction for differences in R_0 between constructs. The forces for the indicated 57-mer data points are beyond the upper bound, as the corresponding E^*_{FRET} values were below the calibration range of our optical force sensor.

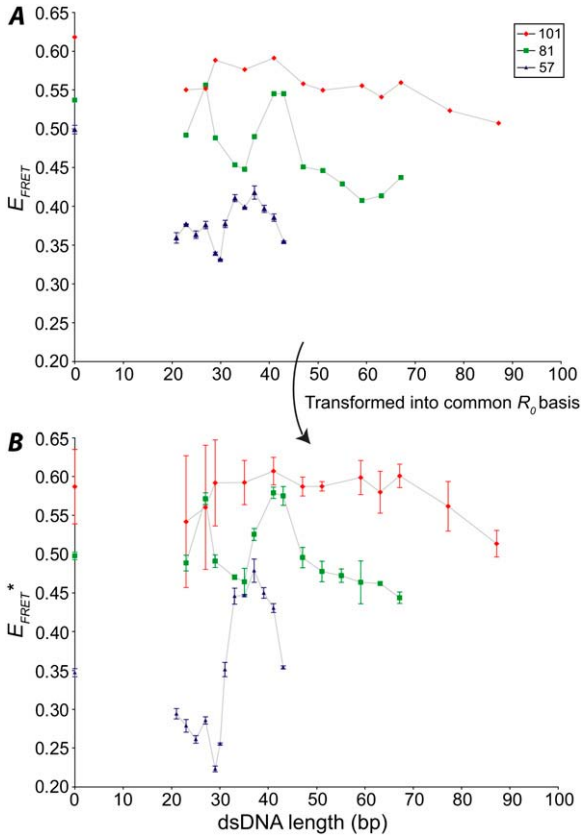

FIGURE 2 (*A*) FRET efficiencies for each construct as a function of complement length. Experimental data are shown as individual points; the lines between points are shown only to guide the eye. The 57-mer data are from five independent measurements; means and SD are shown. Most 81 and 101 measurements were repeated at least once. (*B*) Corresponding FRET efficiencies when transformed into a common R_0 basis.

Instead, E_{FRET} changed nonmonotonically as a function of increasing dsDNA length for all three loop lengths, with the magnitude of the nonmonotonicity most pronounced for the 81- and 57-base loops. An overall downward trend of E_{FRET} versus dsDNA length is evident in the 101- and 81-base loops, but both 81- and 57-base loops displayed pronounced local maxima. Although there may appear to be a ''period'' in the 81- and 57-base loops suggestively similar to the helical repeat of canonical B-DNA (10.5 bp), a power spectrum analysis reveals no strong signal (data not shown). We note that any periodic component in the FRET signal (presumably arising from dsDNA helicity) would be convolved with several aperiodic components and thus would be unlikely to show a strong signal in such an analysis.

It was possible that the nonmonotonic trends we observed were caused by photophysical variations of the FRET dyes between the different constructs. Such variations could result in different values of the Förster radius, R_0, which would consequently result in different values of E_{FRET} for each construct. To address this issue, we measured the fluorescence quantum yield and overlap integral for each experimental construct as well the fluorescence anisotropy for many 57-base loop constructs (Supplementary Figs. S4–S6). There was little variation from construct to construct except for the 57-base loop with small n_D (the number of double-stranded DNA bp). These data were used to calculate E^*_{FRET}, an approximation of E_{FRET} corrected for differences in R_0 (Fig. 2 *B*, see the Supplementary Material for details of the calculation). The overall trends in our data are unaffected by corrections for differences in R_0.

We next examined the role of possible ssDNA artifacts. We attempted to preclude secondary structure formation in the ssDNA region by appropriate sequence design. Nevertheless, ssDNA is a complicated polymer with significant nonlocal interactions when weakly stretched and with sequence-dependent mechanical properties (19). We constructed an analog of the 57-base loop with a PEG-based linker (Supplementary Material) replacing ssDNA between the two fluorophores. The inert PEG linker prevents nonlocal interactions (e.g., secondary structure formation) within the force sensor and between the force sensor and other elements of the construct. The length of the PEG linker was chosen to replicate the contour length of the ssDNA sensor as closely as possible.

The goals of these control experiments were not to perform a quantitative force comparison with the ssDNA-based sensor (which is not possible because we lack the required empirical force-versus-E_{FRET} curve for the PEG-based sensor) but to validate the ability of ssDNA to measure force in this geometry and to compare the overall shape of the curves. We found that the E_{FRET}-versus-dsDNA length curve for the PEG-based sensor had a strikingly similar pattern to the curve obtained for the ssDNA-based sensor (Fig. S3 and Supplementary Material). The similarity between these patterns suggests that the ssDNA-based force sensor indeed measures the mechanics of the ss/dsDNA material outside the sensor region and that the pattern we observe is not simply a result of nonlocal interactions within the force-sensing region. These experiments do not rule out nonlocal interactions involving the remaining ssDNA (between the force sensor and the ds region), which would be expected to be most prominent in larger loops and shorter dsDNA lengths.

Rationalizing FRET data with molecular models

FRET measurements report on force experienced by the ssDNA sensor, but they do not provide a detailed view of microscopic structure in either single-stranded or double-stranded regions of our loop constructs. To infer such details from our data, we have explored the statistical mechanics of several microscopic models for ssDNA and dsDNA. Predictions of these models clarify the possible contributions of DNA flexibility, helicity, excluded volume, and force-induced melting to the observable quantity E_{FRET}.

DNA models with different levels of microscopic resolution offer distinct advantages. At one extreme, atomically

detailed representations include all classical degrees of freedom whose energetics and thermal fluctuations could shape mechanical response. Computational requirements, however, typically restrict the study of such models by molecular dynamics to small DNA molecules (usually dodecamers, although larger constructs have recently been simulated (20)) and short time scales (hundreds to thousands of nanoseconds). The size of our DNA constructs precludes gathering statistically meaningful results from this approach. In contrast, reduced models, which explicitly represent only a subset of microscopic degrees of freedom, permit exhaustive statistical characterization. Moreover, the effects of incorporating or omitting specific fluctuations can help reveal their importance and susceptibility to forces. Coarse-grained models for DNA at the level of individual bp have been employed in many contexts (21), notably for rationalizing results of cyclization experiments described in the Introduction (22).

Because dsDNA segments of our constructs are shorter than a single persistence length, and ssDNA segments are much longer than their own persistence length, the crudest coarse-grained model would represent the double-stranded region as a rigidly straight rod, and the single-stranded region as an ideal random walk connecting the rod's ends. As n_D increases in this model, the single-stranded region becomes both shorter and more highly strained, leading to a monotonic increase in fluorophore separation and a concomitant decrease in E_{FRET}. This model (details presented in the Supplementary Material) captures the generally downward trend of E_{FRET} as a function of n_D for the 101- and 81-base loops, but its numerical predictions contrast dramatically with experiment for large n_D (Fig. 3, *rigid rod*). In that limit, rigidly straight dsDNA corresponds to nearly vanishing E_{FRET}, whereas measured values do not fall below 0.3 for any construct. Substantial energy transfer for large n_D thus indicates that the molecules we generated, as designed, are under sufficient force to induce appreciable curvature in the dsDNA helical axis.

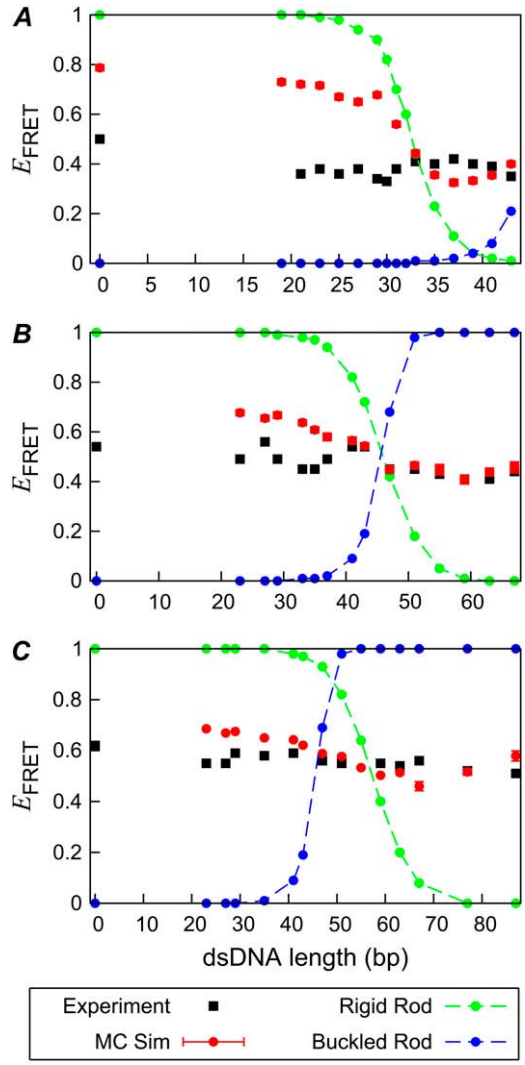

FIGURE 3 Detailed behavior of E_{FRET} as a function of complement length, experiments, and model predictions. Shown are experimental data (*black squares*), simple analytic models (buckled rod, *blue lines*; rigid rod, *green lines*), and MC simulations (*red points*, mean ± 2 SE). Both analytic and simulation results use R_0 inferred from photophysical measurements for each construct: (*A*) 57-base loop, (*B*) 81-base loop, and (*C*) 101-base loop. The *x* and *y* axis scales are identical for each panel.

Buckling of dsDNA generates nonmonotonic E_{FRET} even in simple models

Moving beyond the rigid rod model for our loop constructs requires a quantitative description of dsDNA bending. The WLC (23), a fluctuating elastic rod of fixed contour length, is a common and reasonable choice for this purpose. Under compression, a short WLC segment acts much as a zero-temperature elastic rod. In particular, it buckles with high probability under compressive forces greater than a threshold value (24) and becomes extremely susceptible to additional force. Although attachment of ssDNA will additionally apply shear forces to the double helix, our estimates suggest that they are small in magnitude relative to compressive forces (see the Supplementary Material); we neglect their effects in this discussion. The Euler buckling force decreases with a chain's contour length, so that longer stretches of buckled dsDNA are in fact softer than shorter stretches. This fact underlies a surprising prediction of the WLC model for our experiments (see the Supplementary Material): when the internal force of a loop is sufficient to appreciably bend the double-stranded segment, E_{FRET} is an increasing function of n_D (Fig. 3, *buckled rod*).

Although our experimental data exhibit ranges of n_D over which E_{FRET} increases, none of the constructs crosses over from decreasing to increasing E_{FRET} in a way that would signal an abrupt buckling transition. Nevertheless, the physics of buckling strongly shapes the behavior of more sophisticated models, whose predictions for large n_D agree quite well with our measurements.

Statistical mechanics of backbone bending and helix twisting explain several prominent features of our data for loops under high force

The most detailed representation of DNA we considered resolves the spatial arrangement of bases, the chemical linkage of FRET fluorophores, and helicity of the double-stranded region. Finer aspects of molecular structure appear only implicitly, as in the local susceptibility of ssDNA to bending and of dsDNA to bending and twisting. Using Monte Carlo methods, we thoroughly sampled thermal fluctuations of this model for each loop construct investigated in the laboratory. From histograms of fluorophore separation, we calculated E_{FRET} according to standard formulas (see the Supplementary Material).

With no free parameters, these WLC calculations capture both the scale of E_{FRET} and its weak dependence on n_D for all three loops at higher dsDNA lengths (Fig. 3). These results do not significantly change after correcting for variations in R_0 across constructs (Fig. S8). Although these numerical results manifest asymptotic trends suggested by the simpler models described above, they agree with the experiments much more favorably for all values of n_D and for all loop sizes. Details described by our computational model but neglected in those simple calculations (including dsDNA helicity and the size of fluorophore linkers) thus influence E_{FRET} considerably. The scale of variations in E_{FRET} captured by our simulations of 81- and 101-base loops, with no free parameters (Fig. 3, *B* and *C*), matches the experimental data with an accuracy rarely achieved for numerical prediction of E_{FRET} in biophysical systems. Calculated E_{FRET} deviates from measurements most noticeably for instances of the 57-base loop under weak forces (Fig. 3 *A*). Because these constructs are comprised mainly of ssDNA, and their internal forces are not expected to bend dsDNA appreciably, we attribute the deviations to a neglect of nonlocal attractions between different regions of ssDNA.

A simple model of dsDNA twist predicts local maxima in E_{FRET} at integer multiples of the helical repeat n_{rot} and local minima at half-integer multiples (see the Supplementary Material). Our FRET measurements for the short loop exhibit an oscillatory component with a period suggestively similar to n_{rot} (Fig. 2). In contrast to our model and our simulations, however, the E_{FRET} maxima of this component do not lie at integer multiples of n_{rot} but instead at half-integer multiples. This discrepancy could result from dynamic fraying of the ends of the ds regions, which has been observed by NMR (25). Control experiments with Exonuclease I (which degrades ssDNA) were able to neither confirm nor preclude the presence of fraying (data not shown). If such fraying is present, it can be approximated as converting end dsDNA bp into ssDNA and would shift our simulation curve to larger n_D by the number of frayed bases.

dsDNA does not appear to melt with high probability under sharp bending

Results of some cyclization experiments discussed in the Introduction have been interpreted to indicate that dsDNA responds to compressive force by ''bubbling'' or locally ''melting'' (10). The possibility of such melting is notably absent in our models, which assume complete hybridization of loop and complement. When one basepair within the ds region was converted to unpaired single bases in our model, calculated E_{FRET} increased considerably (from 0.39 to 0.52 for the 57-base loop with 39-nt complement, data not shown), degrading agreement with experiment.

Melting can be similarly imposed in experiments by use of strands of DNA that are not entirely complementary to the loop. If melting occurred with high probability in perfectly complementary constructs, then introducing mismatched bases at likely melting sites should not change E_{FRET} significantly. On the contrary, forced melts at the center of the 39-base ds region of our shortest, most strained loop (57-base) greatly increased E_{FRET}, corresponding to a reduction of force in the loop (Fig. 4 *A*). E_{FRET} increased from 0.40 (no defect) to 0.49 (three-base defect), and the corresponding forces dropped from 4.8 ± 1.3 pN (no defect) to 3.9 ± 1.1 pN (three-base defect). The force for the three-base mismatch construct is lower than any forces determined for the defect-free constructs of the same loop length (Fig. 1 *C*). This fact suggests that Watson-Crick basepaired DNA can withstand relatively high compressive forces ($>$20 pN) without sustained multibase unpairing like that expressly engineered into our controlled three-base defect construct.

No evidence for melting transitions on a wide range of timescales

These results give us qualitative information about the relative probabilities of fully basepaired and melted conformations, but they do not address the absolute time scales of melting and hybridization. When these interconversions occur, they should produce dynamic fluctuations in fluorescence intensity. Single-molecule FCS measures the time correlation function of such intensity fluctuations, which should decay on the timescale of interconversion kinetics. Previous FCS experiments have found relaxation lifetimes for B-DNA melting in the range of 30–100 μs (26), whereas NMR experiments found lifetimes on the order of 0.5–50 ms (27).

With an instrument similar to those previously reported (28), we investigated the same 57-base loop with 39-base ds region studied in Fig. 4 *A*. Fluctuations in fluorescence intensity from our constructs arise from two sources: the diffusive fluctuations of molecules as they enter and exit the excitation volume and fluctuations from conformational changes in the molecules themselves. The diffusive fluctuations were accounted for by measuring the autocorrelation function for control loops with only one (donor) dye, $G_{1D}(\tau)$. Dividing the autocorrelation function for the loops with both dyes, $G_{BD}(\tau)$, by $G_{1D}(\tau)$ gave the contribution from conformational dynamics (such as from melting/hybridizing) in our loops.

We did not detect decay of fluorescence intensity correlations on time scales accessible to our instrument: specifically,

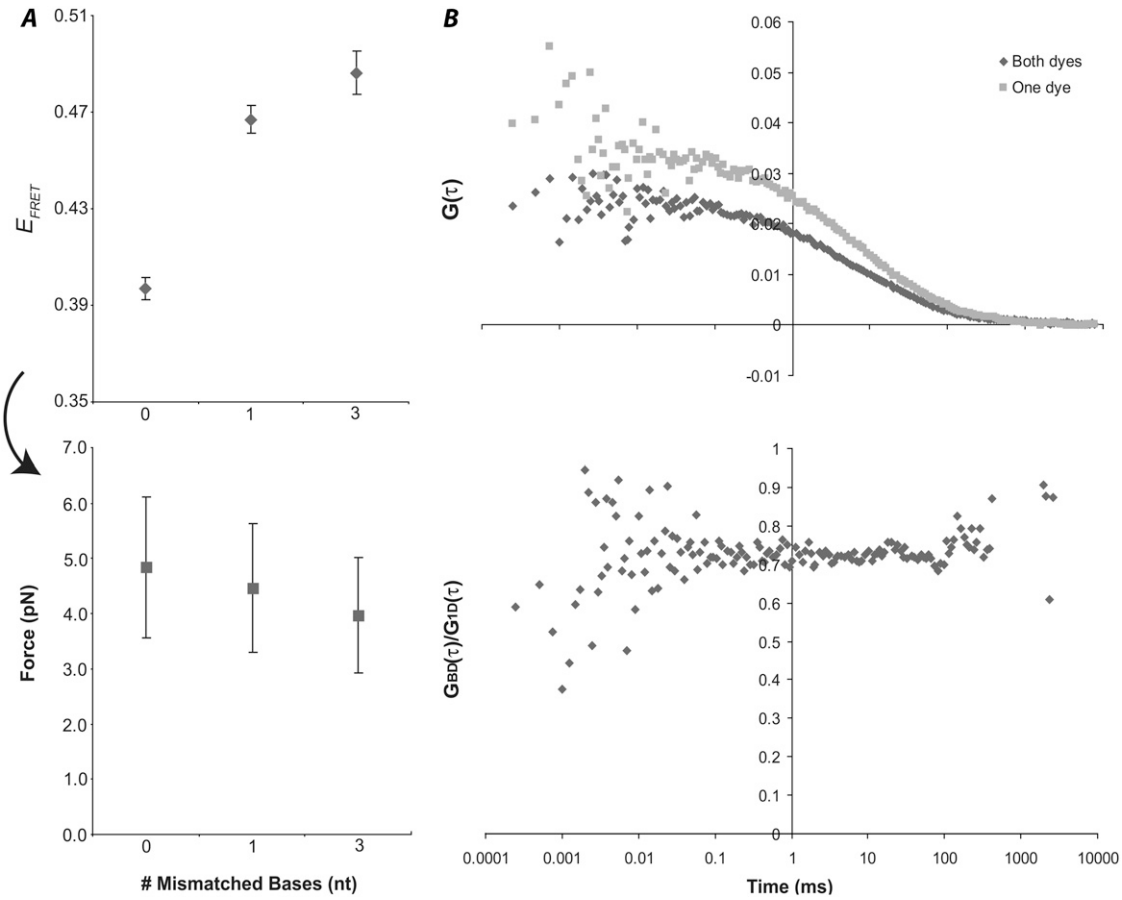

FIGURE 4 Engineered melt and transient melt experiments. (*A*) FRET efficiency (*top*) and force (*bottom*) measurements for 57-mer loop, 39-base annealed construct with 0, 1, or 3 base mismatches. Mean ± SD are shown for five independent measurements. (*B*) FCS measurements. (*Top*) Autocorrelation functions for 57-mer loop, 39-base annealed complement with both or one dye attached. (*Bottom*) Division of autocorrelations.

the quotient of autocorrelation functions $G_{BD}(\tau)/G_{1D}(\tau)$ (Fig. 4 *B*, *top*), was constant over the timescales 1–1000 μs (Fig. 4 *B*, *bottom*). The sum of melting and hybridization rates therefore falls well outside the range previously reported for unstrained dsDNA. Because the controlled-defect measurements indicate a low probability of melts, a large increase in relaxation rate would require dramatically accelerated hybridization kinetics, which seems unlikely under large strain. Bending DNA therefore appears to slow these conformational transitions at least 10-fold without a strong bias for melting over hybridization.

CONCLUSIONS

In this article, a new method for both applying and reading out forces in short stretches of DNA is presented. Molecules comprising mainly dsDNA experience large forces under cyclization, registering forces in the range 3 pN (for the longest loop of 101 bases) to >20 pN (for the shortest loop of 57 bases). Dependence of these forces on loop length is consistent with the statistical mechanics of a simple WLC model for fluctuations in DNA conformation. Bending-induced disruption of basepairing in dsDNA is therefore not needed to explain the magnitude of internal forces that develop in short-loop constructs.

For each loop length, force developed in a complicated way with increasing fraction of dsDNA. Irregular base-to-base variations suggest an intriguing sensitivity to nucleotide sequence, which could be exploited to study sequence-dependent bending rigidity (29). Nonmonotonic trends in force as a function of complement length mirror the modulation of computed forces by backbone twisting around the helical axis of dsDNA.

The quantitative connections we have established between experiment and theory are not trivial consequences of loop geometry, as illustrated by the failure of simple mechanical estimates. Only by thoroughly sampling the range of thermal fluctuations in dsDNA conformation could we reasonably reproduce measured values of FRET efficiency. A better account of detailed variations in force might be obtained from a more elaborate model that includes nonlocal ssDNA interactions, sequence-dependent elasticity, bending anisotropy,

and twist-bend coupling, as well as fraying and low-probability melting events. The coarse description we have employed, lacking any freely adjustable parameters, is nonetheless a remarkably successful representation given the short length scales and high forces involved.

The methodology presented here may prove generally useful in studying the effect of substrate prestrain on DNA binding proteins. Although the effect of substrate-induced strain has been studied for some systems (30,31), the ability to ''dial in'' a specific amount of prestrain into the substrate is still desirable. Introduction of a binding site would allow each of the constructs that we studied to provide a unique prestrained substrate to a DNA binding protein and may also permit studies of the effect of substrate tension on the mechanochemistry of molecular machines.

SUPPLEMENTARY MATERIAL

To view all of the supplemental files associated with this article, visit www.biophysj.org.

This work is dedicated to Nicholas Cozzarelli, who prompted our studies of strained DNA.

H.S. thanks the Fannie and John Hertz foundation. D.S. acknowledges support from Department of Defense—National Defense Science and Engineering Graduate Fellowship Program—and National Science Foundation predoctoral fellowships.

This work was supported in part by the University of California, Berkeley, the Hellman Faculty Fund, the Sloan and Searle Foundations, and the Department of Energy Office of Science, Energy Biosciences Program KC0304, DE-AC03-76SF00098. We thank Jon Widom for extensive feedback and helpful discussions, Sander Pronk and Arthur Edelstein for fruitful discussions, and the Marqusee and Bustamante labs for the use of their equipment.

REFERENCES

1. Perez-Martin, J., F. Rojo, and V. de Lorenzo. 1994. Promoters responsive to DNA bending: a common theme in prokaryotic gene expression. *Microbiol. Rev.* 58:268–290.
2. Vilar, J. M., and L. Saiz. 2005. DNA looping in gene regulation: from the assembly of macromolecular complexes to the control of transcriptional noise. *Curr. Opin. Genet. Dev.* 15:136–144.
3. Richmond, T. J., and C. A. Davey. 2003. The structure of DNA in the nucleosome core. *Nature*. 423:145–150.
4. Rice, P. A., S. W. Yang, K. Mizuuchi, and H. A. Nash. 1996. Crystal structure of an IHF-DNA complex: A protein-induced DNA U-turn. *Cell*. 87:1295–1306.
5. Bustamante, C., S. B. Smith, J. Liphardt, and D. Smith. 2000. Single-molecule studies of DNA mechanics. *Curr. Opin. Struct. Biol.* 10: 279–285.
6. Smith, S. B., Y. J. Cui, and C. Bustamante. 1996. Overstretching B-DNA: The elastic response of individual double-stranded and single-stranded DNA molecules. *Science*. 271:795–799.
7. Cloutier, T. E., and J. Widom. 2004. Spontaneous sharp bending of double-stranded DNA. *Mol. Cell.* 14:355–362.
8. Cloutier, T. E., and J. Widom. 2005. DNA twisting flexibility and the formation of sharply looped protein-DNA complexes. *Proc. Natl. Acad. Sci. USA*. 102:3645–3650.
9. Wiggins, P. A., and P. C. Nelson. 2006. Generalized theory of semiflexible polymers. *Phys. Rev. E Stat. Nonlin. Soft Matter Phys.* 73:031906.
10. Yan, J., and J. F. Marko. 2004. Localized single-stranded bubble mechanism for cyclization of short double helix DNA. *Phys. Rev. Lett.* 93:108108.
11. Du, Q., C. Smith, N. Shiffeldrim, M. Vologodskaia, and A. Vologodskii. 2005. Cyclization of short DNA fragments and bending fluctuations of the double helix. *Proc. Natl. Acad. Sci. USA*. 102: 5397–5402.
12. Crothers, D. M., J. Drak, J. D. Kahn, and S. D. Levene. 1992. DNA bending, flexibility, and helical repeat by cyclization kinetics. *Methods Enzymol.* 212:3–29.
13. Lang, M. J., and S. M. Block. 2003. Resource Letter: LBOT-1: Laser-based optical tweezers. *Am. J. Phys.* 71:201–215.
14. Fisher, T. E., A. F. Oberhauser, M. Carrion-Vazquez, P. E. Marszalek, and J. M. Fernandez. 1999. The study of protein mechanics with the atomic force microscope. *Trends Biochem. Sci.* 24:379–384.
15. Shroff, H., B. M. Reinhard, M. Siu, H. Agarwal, A. Spakowitz, and J. Liphardt. 2005. Biocompatible force sensor with optical readout and dimensions of 6 nm^3. *Nano Lett.* 5:1509–1514.
16. Ha, T., T. Enderle, D. F. Ogletree, D. S. Chemla, P. R. Selvin, and S. Weiss. 1996. Probing the interaction between two single molecules: fluorescence resonance energy transfer between a single donor and a single acceptor. *Proc. Natl. Acad. Sci. USA*. 93:6264–6268.
17. Clegg, R. M. 1992. Fluorescence resonance energy transfer and nucleic acids. *Methods Enzymol.* 211:353–388.
18. Li, G., M. Levitus, C. Bustamante, and J. Widom. 2005. Rapid spontaneous accessibility of nucleosomal DNA. *Nat. Struct. Mol. Biol.* 12: 46–53.
19. Goddard, N. L., G. Bonnet, O. Krichevsky, and A. Libchaber. 2000. Sequence dependent rigidity of single stranded DNA. *Phys. Rev. Lett.* 85:2400–2403.
20. Lankas, F., R. Lavery, and J. H. Maddocks. 2006. Kinking occurs during molecular dynamics simulations of small DNA minicircles. *Structure*. 14:1527–1534.
21. Olson, W. K. 1996. Simulating DNA at low resolution. *Curr. Opin. Struct. Biol.* 6:242–256.
22. Yan, J., R. Kawamura, and J. F. Marko. 2005. Statistics of loop formation along double helix DNAs. *Phys. Rev. E Stat. Nonlin. Soft Matter Phys.* 71:061905.
23. Kratky, O., and G. Porod. 1949. Rontgenuntersuchung geloster Fadenmolekule. *Recl. Trav. Chim. Pays Bas*. 68:1106–1123.
24. Landau, L. D., and E. M. Lifshitz. 1986. Theory of Elasticity. Pergamon Press, Elmsford, NY.
25. Fujimoto, B. S., S. T. Willie, B. R. Reid, and J. M. Schurr. 1995. Position-dependent internal motions and effective correlation times for magnetization transfer in DNA. *J. Magn. Reson. B*. 106:64–67.
26. Altan-Bonnet, G., A. Libchaber, and O. Krichevsky. 2003. Bubble dynamics in double-stranded DNA. *Phys. Rev. Lett.* 90:138101.
27. Gueron, M., and J. L. Leroy. 1995. Studies of base pair kinetics by NMR measurement of proton exchange. *Methods Enzymol.* 261:383–413.
28. Bonnet, G., O. Krichevsky, and A. Libchaber. 1998. Kinetics of conformational fluctuations in DNA hairpin-loops. *Proc. Natl. Acad. Sci. USA*. 95:8602–8606.
29. Coleman, B., W. Olson, and D. Swigon. 2003. Theory of sequence-dependent DNA elasticity. *J. Chem. Phys.* 118:7127–7140.
30. van den Broek, B., M. C. Noom, and G. J. L. Wuite. 2005. DNA-tension dependence of restriction enzyme activity reveals mechanochemical properties of the reaction pathway. *Nucleic Acids Res.* 33:2676–2684.
31. Gemmen, G. J., R. Millin, and D. E. Smith. 2006. Tension-dependent DNA cleavage by restriction endonucleases: Two-site enzymes are ''switched off'' at low force. *Proc. Natl. Acad. Sci. USA*. 103:11555–11560.